Supplementary Information

Rational Synthesis of ZIF-67@Co-Ni LDHs Heterostructure and Derived Heterogenous Carbon-Based Framework as High-Efficient Multifunctional Sulfur Host

Hongtai Li, Quan Jin, Jie Zhao, Bao Wang, Xiaodong Guo,**

Experimental Section

Adsorption and catalytic studies: Mixing sulfur and Li_2S with a molar ratio of 5: 1 in DOL/DME solvent followed by stirring at 60 ℃ for 12 h in Argon-filled gloved box, the Li_2S_6 solution could be obtained. 20 mg GC-Co NPs/ GC-Co@DC-LDO CPs/ GC-Co@DC-LDO YPs/ LDO HPs powders were dispersed individually in 10 mL prepared Li_2S_6 solution with a concentration of 5 mmol L^{-1} based on sulfur, respectively. Observed the color change of these mixtures after standing for 24 h. The supernatants and those precipitates of the mixtures were studied by ultraviolet and visible (UV-vis) spectrophotometry and X-ray photoelectron spectroscopy (XPS), respectively.

The catalytic property was further studied by Cyclic Voltammetry (CV) test of symmetric cells. Mixing annealed products and PVDF with NMP solvents and assembling identical electrodes with a Celgard 2400 membrane as separator, respectively. 20 μL 5 mol L^{-1} Li_2S_8 in DOL/DME (1:1, v/v) electrolyte was added, subsequently. CV was performance on Bio-Logic VMP3 electrochemistry workstation at a scan rate of 50 mV s^{-1} between -1.0 and 1.0 V.

The nucleation and growth of Li_2S from soluble polysulfides were studied by potentiostatic deposition of Li_2S_8 tetraglyme solution (0.2 mol L^{-1} based on sulfur) on CF-based current collectors. About 0.2 mg of GC-Co NPs/ GC-Co@DC-LDO CPs/ GC-Co@DC-LDO YPs/ LDO HPs powders were separately dissolved with ethanol and dispersed on CF papers which were punched into disks with a diameter of 15 mm. 20 μL Li_2S_8 was dropped onto the obtained current collectors as cathode. Lithium foil was employed at the counter electrode, which was separated with cathode by Celgard 2400 membrane and dropped with 20 μL 1 M LiTFSI in DOL/DME (1:1, v/v) on the Li metal side. The cell was galvanostatically discharged to 2.06 V at a constant current density of 0.112 mA, and then kept potentiostatically at 2.05 V for Li_2S nucleation and grew until the

current dropped below 10^{-5}. Evaluated the capacities from deposition of lithium sulfide on various surfaces according to Faraday's law.

Materials characterization: X-ray diffraction (XRD) patterns were obtained by using an X'Pert PRO MDP with Cu Kα radiation (λ= 1.5405Å) with 40 mA and 40 kV. Field emission scanning electron microscopy (FESEM) images were got by using a JEOL JSM-7800F scanning electron microscope operating at 5.0 kV. Transmission electron microscopy (TEM) images were obtained using JEOL JEM-2100F electron microscope operating at 200 kV. X-ray photoelectron spectroscopy (XPS) spectra were recorded using an ESCALAB 250 Xi XPS system of Thermo Scientific, where the base pressure in analysis chamber was 1.5×10^{-9} mbar and the X-ray spot was 500 μm. The nitrogen adsorption-desorption isotherms (at 77 K) were measured on a Quantachrome Autosorb MP sorption analyzer with prior degassing under vacuum at 200 °C for 12 h. Fourier Transform Infrared Spectroscopy (FT-IR) patterns were performed through a T27-Hyperion-Vector22 (Bruker). Raman spectra were performed by an HR-800 (Jobin Yvon). Thermogravimetric analysis-differential thermal analysis (TGA-DTA) data were collected using a DTA-60 (Shimadzu), annealed under air/ N_2 atmosphere at 10 ℃ min^{-1}. A Shimadzu ICPS-7500 inductively coupled plasma optical emission spectroscope (ICP-OES) was used to analyze the contents of metals in samples.

Electrochemical measurements: 70 wt% sulfur composites mentioned above, 20 wt% super P, and 10 wt% PVDF were mixed to form a homogeneous slurry using NMP as the dispersant. Then the black slurry was coated on an aluminum foil collector and dried at 60 ℃ under vacuum overnight to obtain cathodes. Coin cells (CR 2032) were assembled in an Argon-filled glovebox with a lithium foil as the anode, Cellgard 2400 as the separator and 1 M LiTFSI + 2.0% $LiNO_3$ dissolved in DOL/DME (1:1, v/v) as the electrolyte. The electrolyte amount was calculated with the electrolyte/ sulfur ratio of 15:1 (μL mg_s^{-1}). The electrode area was 1.77 cm^2 (diameter of 15 mm). The areal mass loading on the electrode was about 1.0-1.3 mg cm^{-2} besides the thick electrode was 2.4 mg cm^{-2} for high sulfur loading cycle stability test with 0.5 C. The electrochemical performance of electrodes was evaluated by galvanostatic cycling in 2032 type coin cells using a LANHE-

CT2001A analyzer at different current densities with a potential window of 1.7-2.8 V vs. Li^+/Li. CV was tested on a Bio-Logic VMP3 electrochemistry workstation from the voltage of 1.7-2.8 V vs. Li^+/Li with the scan rate from 0.1 to 0.5 mV s^{-1}. For Galvanostatic Intermittent Titration Technique (GITT) tests, a constant current density of 0.05 C was adopted for 30 min followed by a pulse of duration of 2 h to collect the potential response. Electrochemical Impedance Spectroscopy (EIS) analyses were carried out in the range of 100 kHz to 0.01 Hz. The specific capacities were calculated according to the loading mass of sulfur in the cathodes.

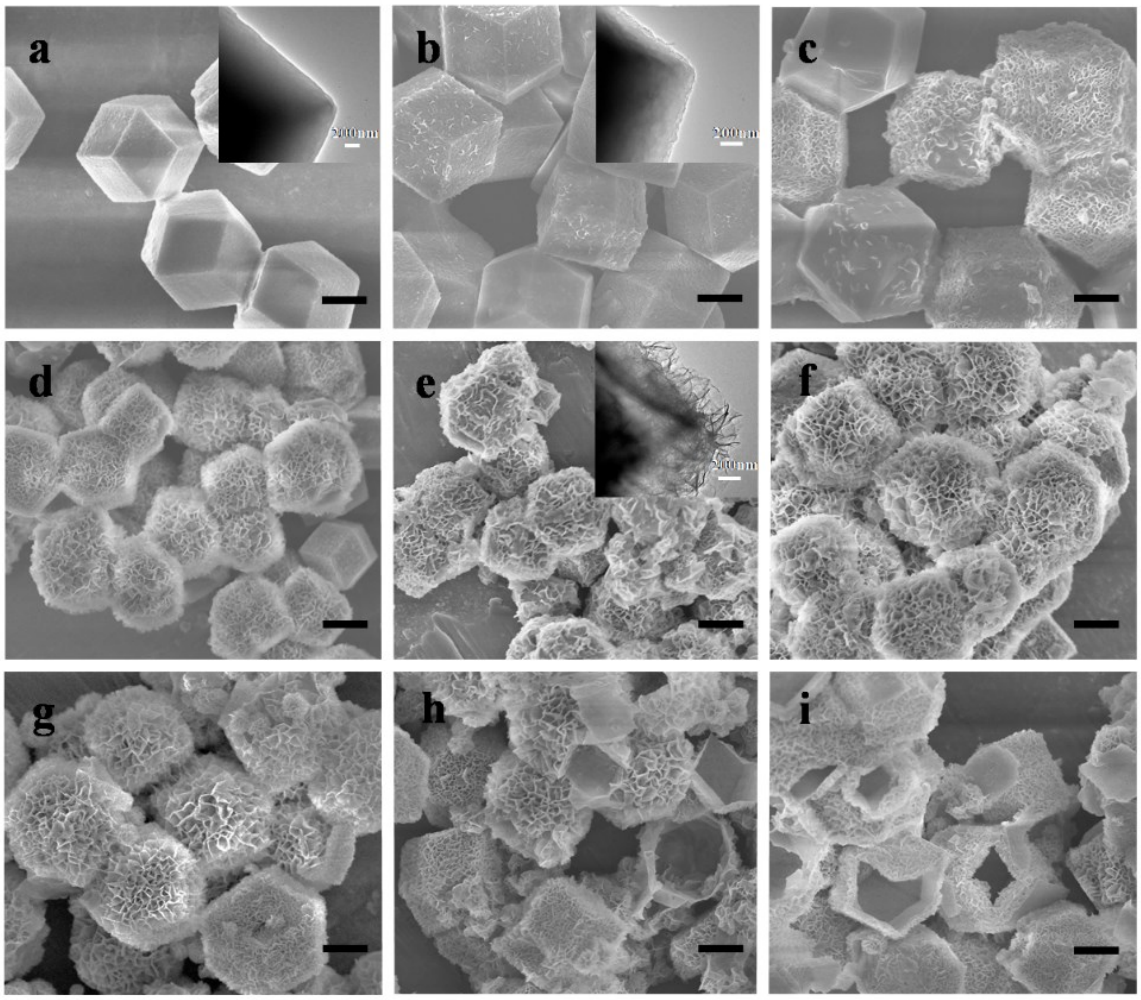

Figure S1. FESEM images of as-synthesized ZIF-based products after different solvothermal durations: (a) 0.5 h, (b) 1 h, (c) 1.5 h, (d) 2 h, (e) 3 h, (f) 4 h, (g) 9 h, (h) 12 h, (i) 24 h. Inset of panel (a), (b) and (e) are the corresponding magnified TEM images. Scale bar: 2μm.

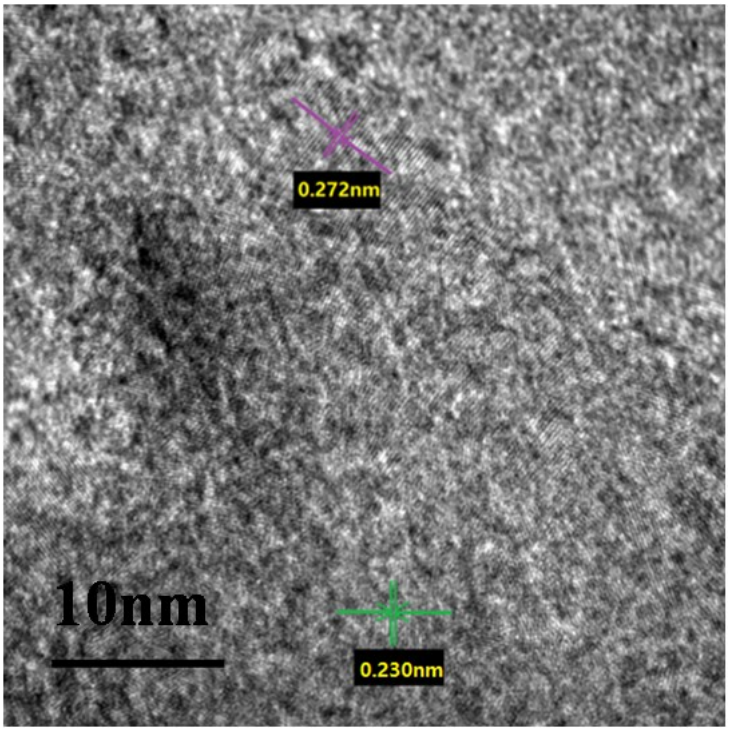

Figure S2. High-resolution TEM image of H-LDH.

The lattice spacings of 0.230 and 0.272 nm are indexed to the (015) plane of the nickel hydroxide hydrate (PDF# 38-0715) and cobalt hydroxide (PDF# 02-0925), respectively.[1]

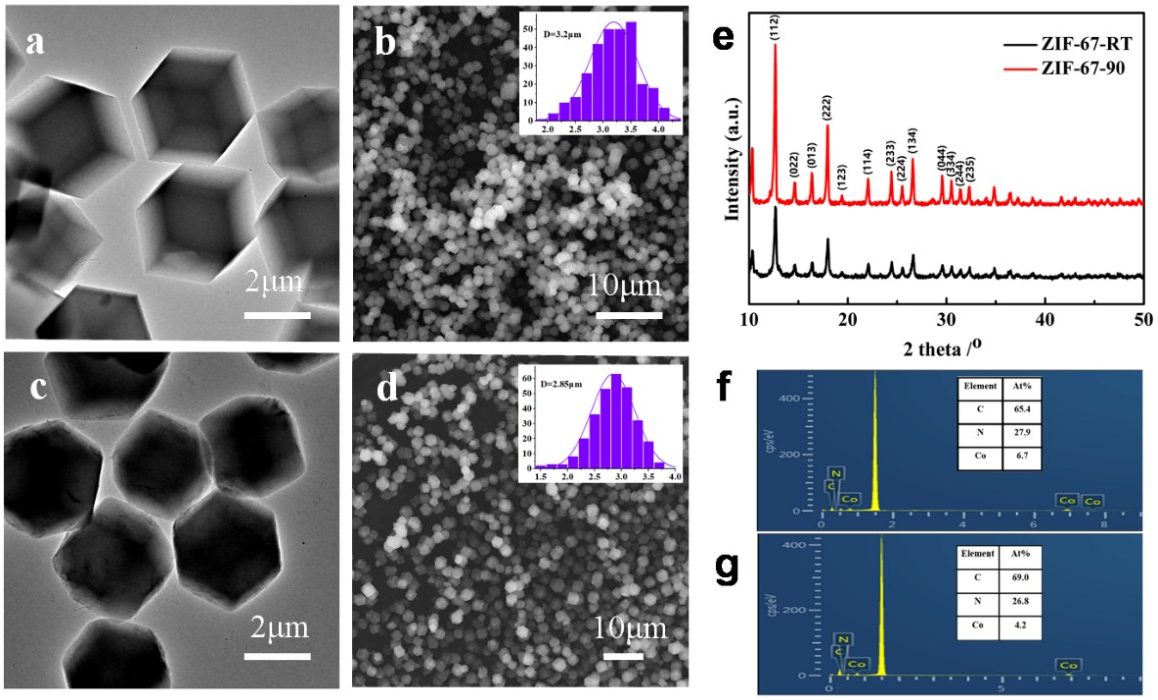

Figure S3. TEM images of (a) ZIF-67-90; (c) ZIF-67-RT; FESEM images and corresponding size distribution of ZIF-67 crystals of (b) ZIF-67-90; (d) ZIF-67-RT; (e) XRD patterns; EDX patterns of (f) ZIF-67-90 and (g) ZIF-67-RT. The highest peak arises from the substrate of Al foil for SEM observation.

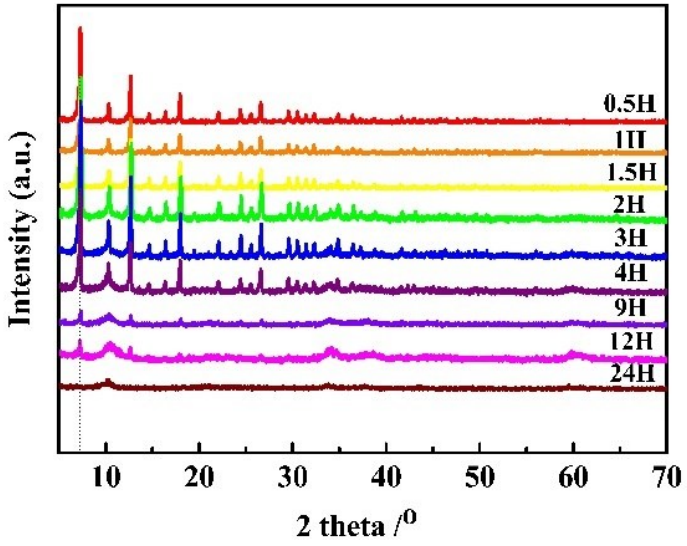

Figure S4. (a) XRD patterns of the as-synthesized ZIF-based products with different solvothermal durations (0.5, 1, 1.5, 2, 3, 4, 9, 12, and 24 h); (b) selected enlarged portion the as-synthesized ZIF-based products with 24 h solvothermal duration and LDH synthesized at room temperature.

The diffraction peaks at 2θ = 10.17°, 22.1°, 33.4° and 59.7° match well with (003), (006), (009), and (110) planes of LDHs.[2]

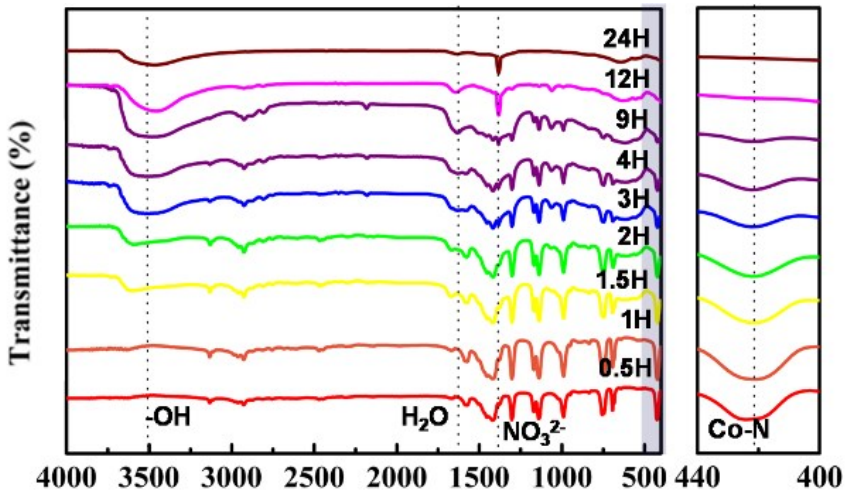

Figure S5. FT-IR spectra of as-synthesized ZIF-based products with different solvothermal durations of 0.5, 1, 1.5, 2, 3, 4, 9, 12, and 24 h.

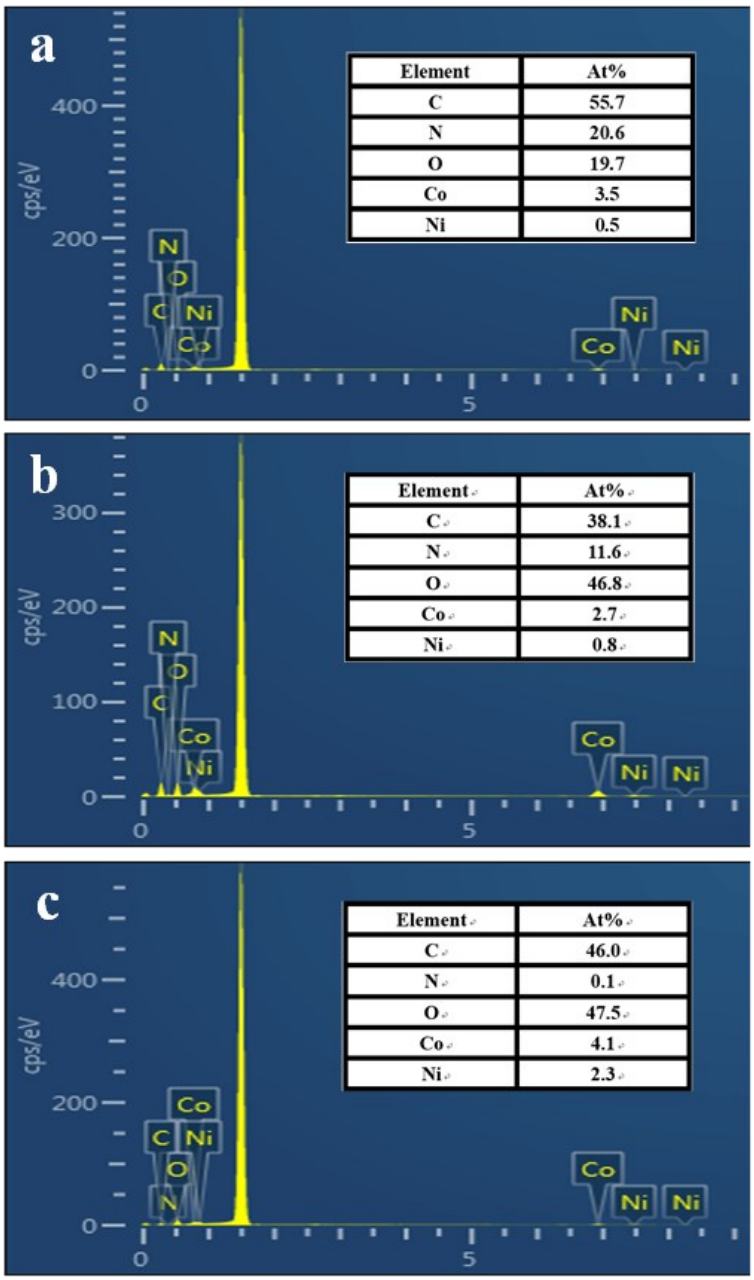

Figure S6. EDX patterns of (a) C-ZIF@LDH, (b) Y-ZIF@LDH, and (c) H-LDH. The highest peak arises from the substrate of Al foil for SEM observation.

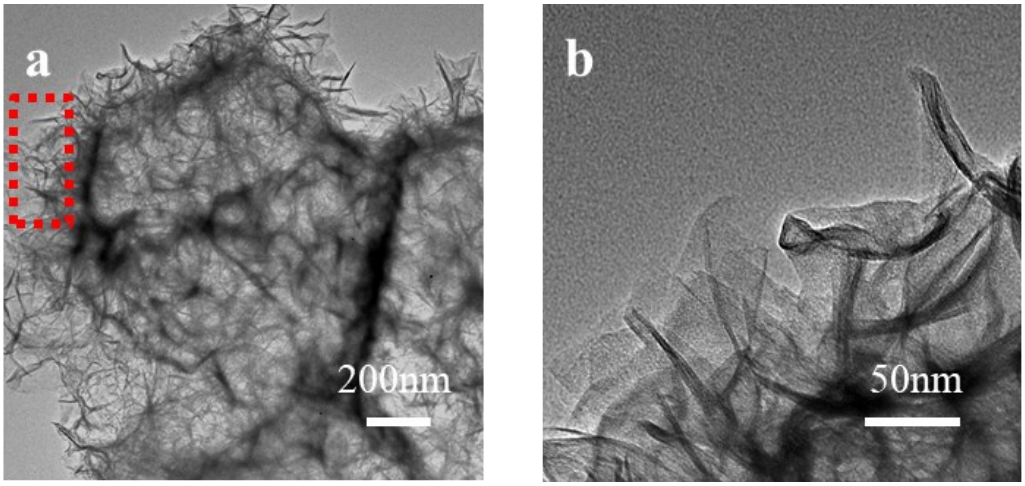

Figure S7. (a, b) TEM images of LDH-RT.

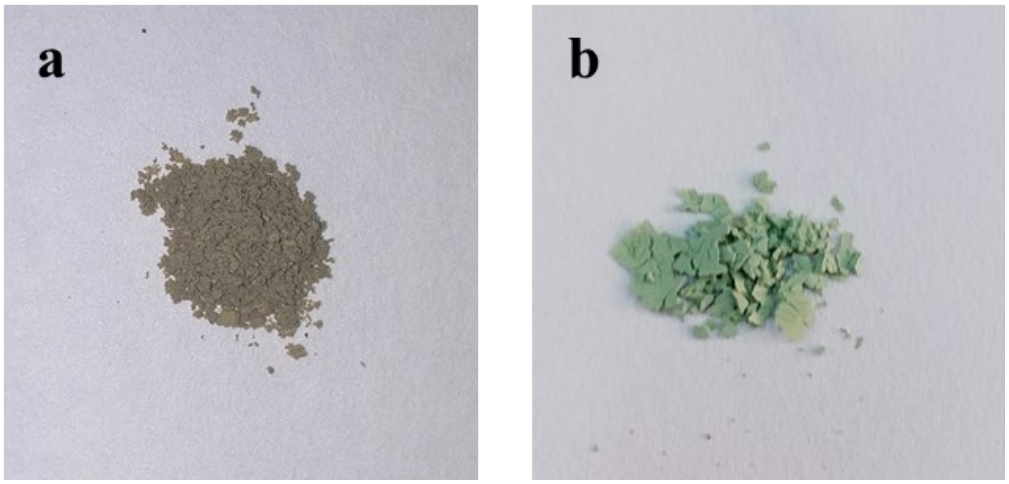

Figure S8. Optical images of (a) H-LDH and (b) LDH-RT.

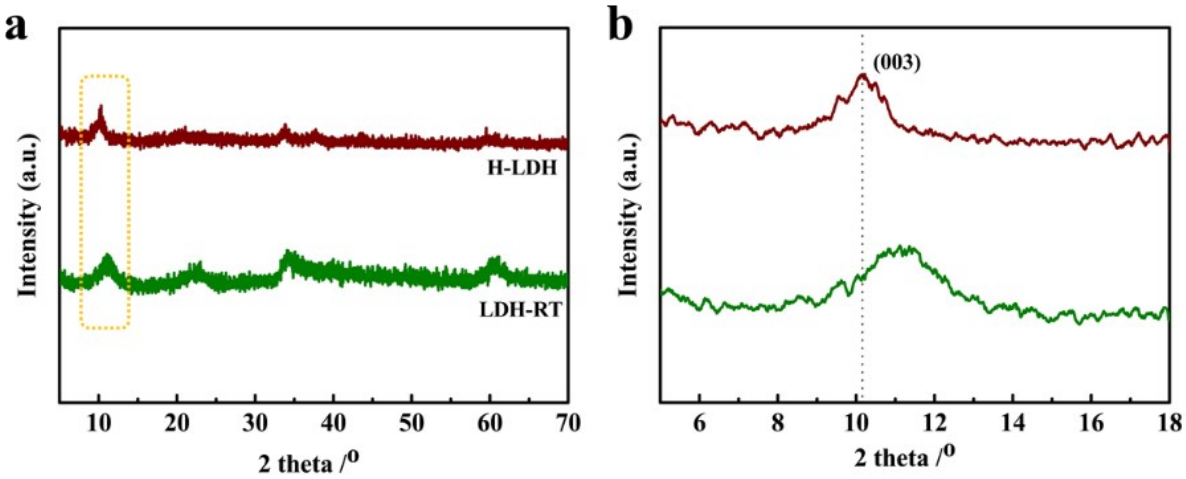

Figure S9. (a, b) XRD patterns and corresponding enlarged part.

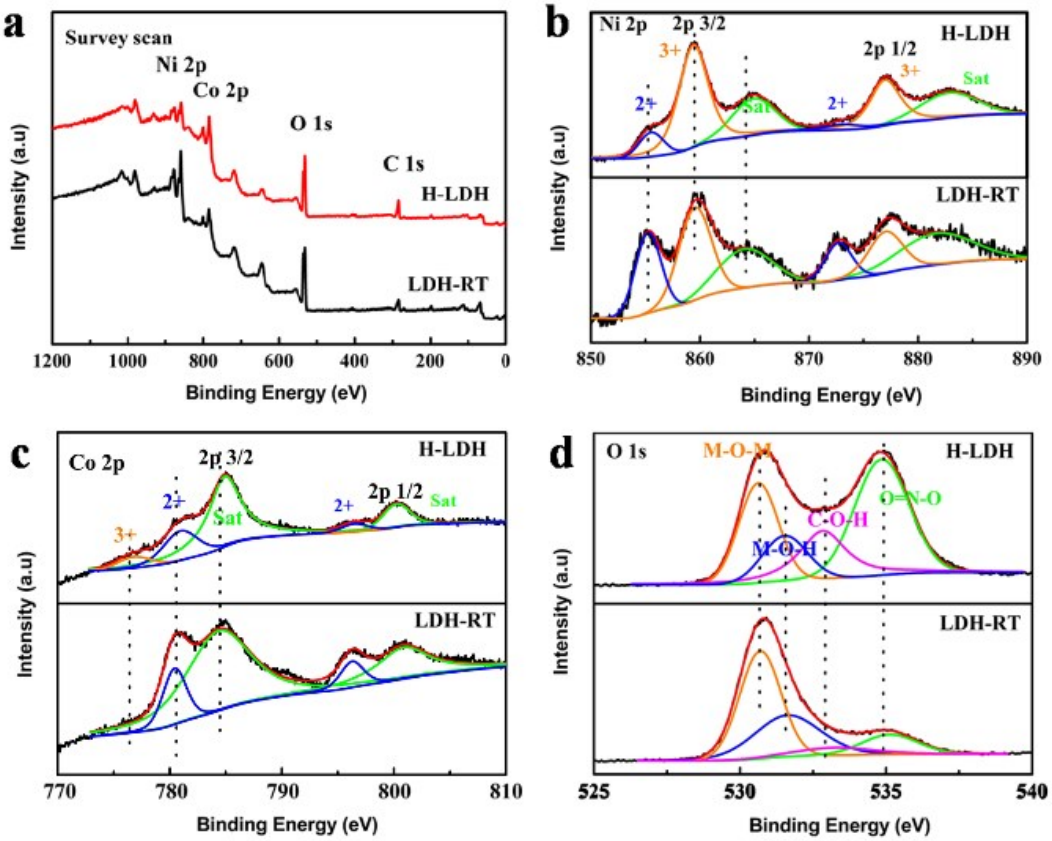

Figure S10. (a) full XPS spectra and (b-d) Ni 2p, Co 2p, O 1s, respectively.

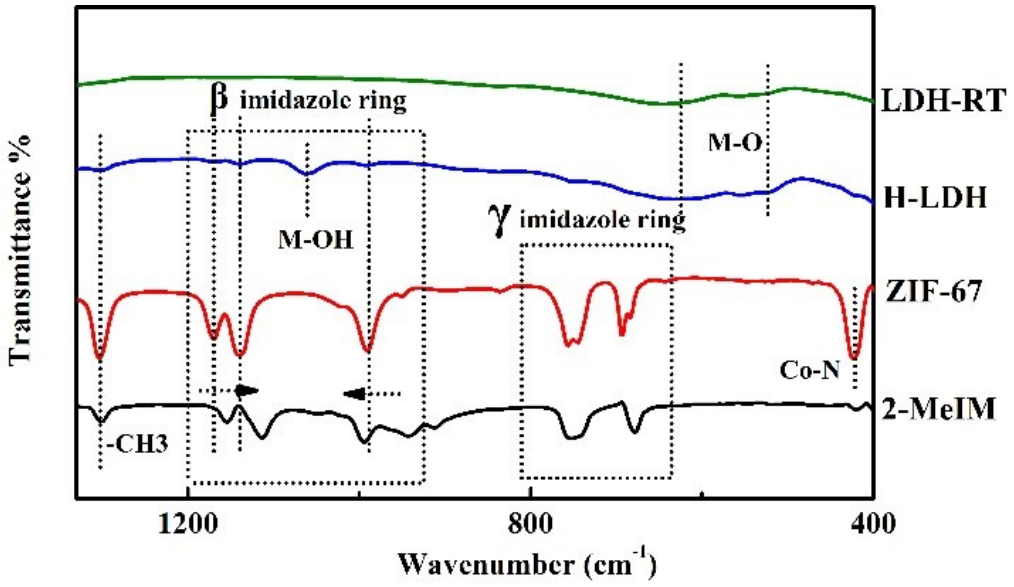

Figure S11. FT-IR spectra of the specific materials.

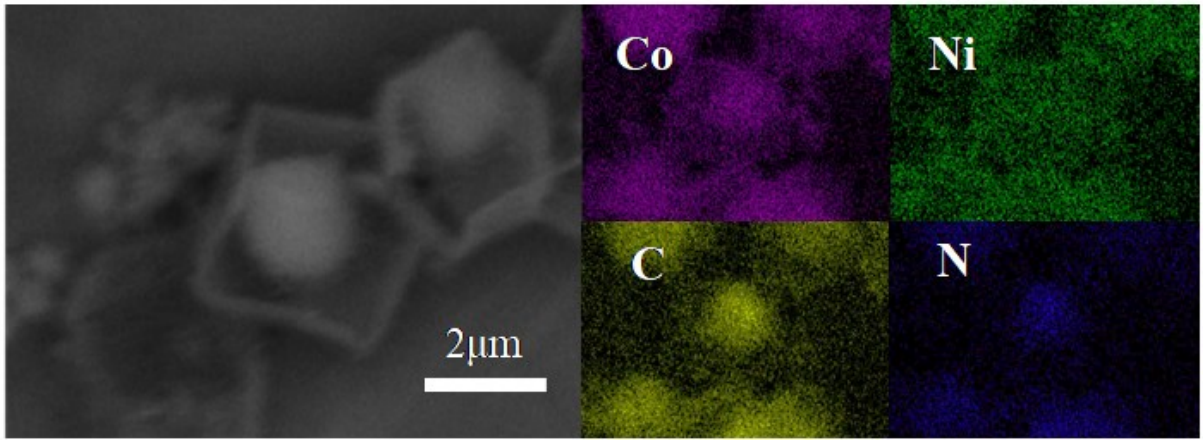

Figure S12. FESEM image and corresponding EDX patterns of a broken GC-Co@DC-LDO YPs.

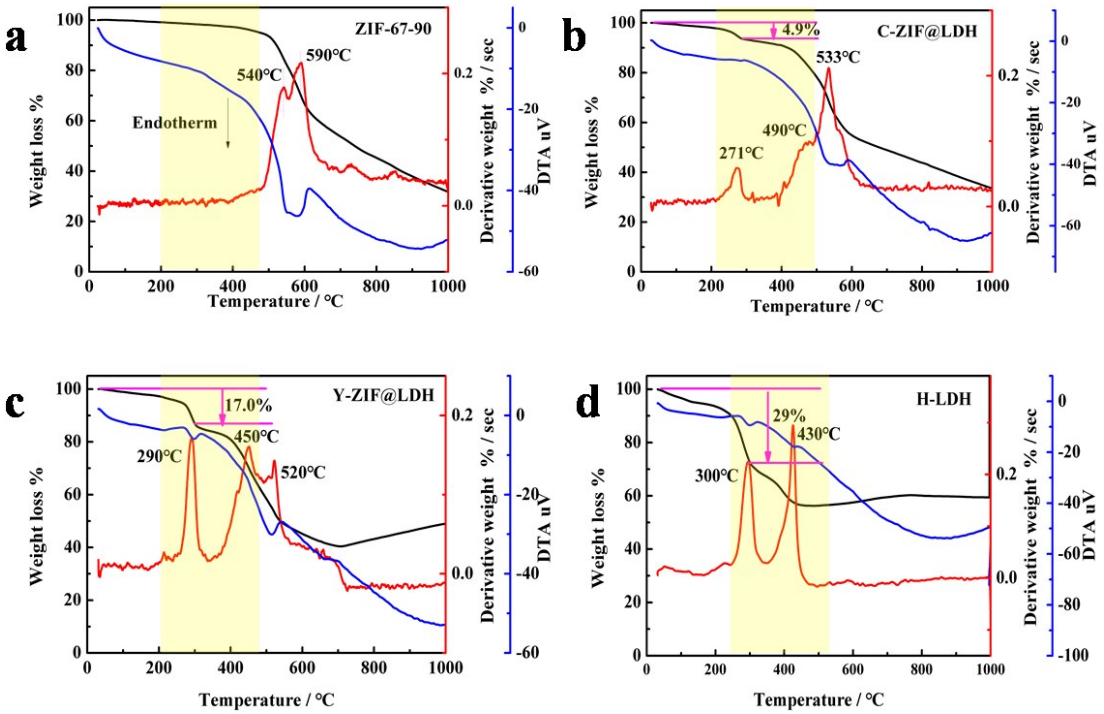

Figure S13. TGA curves of (a) ZIF-67, (b) C-ZIF@LDH, (c) Y-ZIF@LDH, and (d) H-LDH in N_2 atmosphere.

The typical weight loss of ZIF-67 starts from 500 ℃ in N_2 atmosphere, which is attributed to the decomposition of 2-MeIM ligands and formation of Co/C composites.[3]

Co-Ni LDHs experience three weight loss process. In the early stage of TG curve, the slightly slow weight loss is ascribed to the removal of free and adsorbed water.[4] The second step around 300 ℃ is indexed to the dehydroxylation of brucite-like layers. The final step matches the intercalated anions decomposition[5] and Co-Ni LDOs would be obtained as the final product.[6]

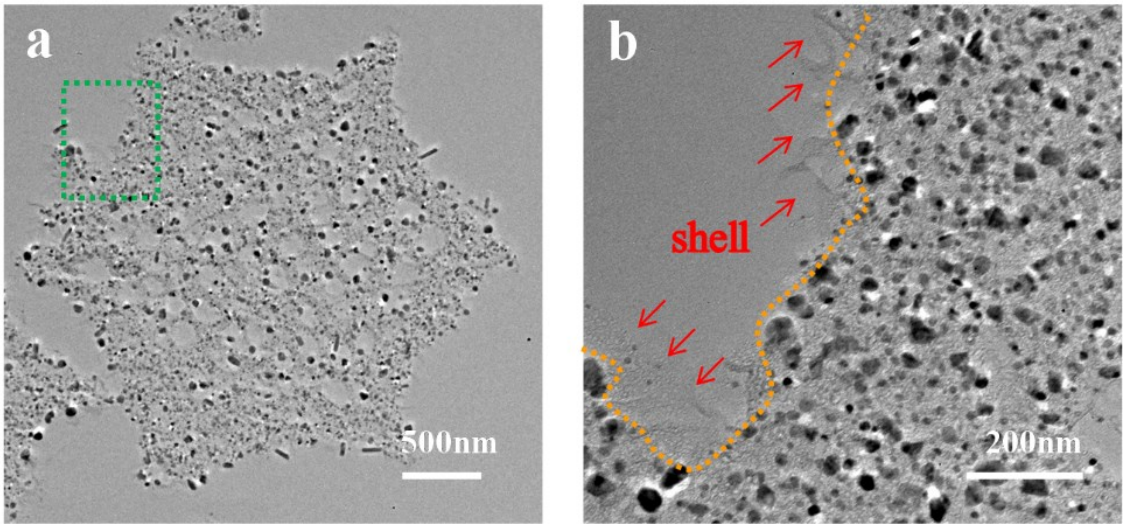

Figure S14. (a) Cross-section TEM image of GC-Co@DC-LDO CPs prepared by ultramicrotomy and (b) coresponding enlarged image.

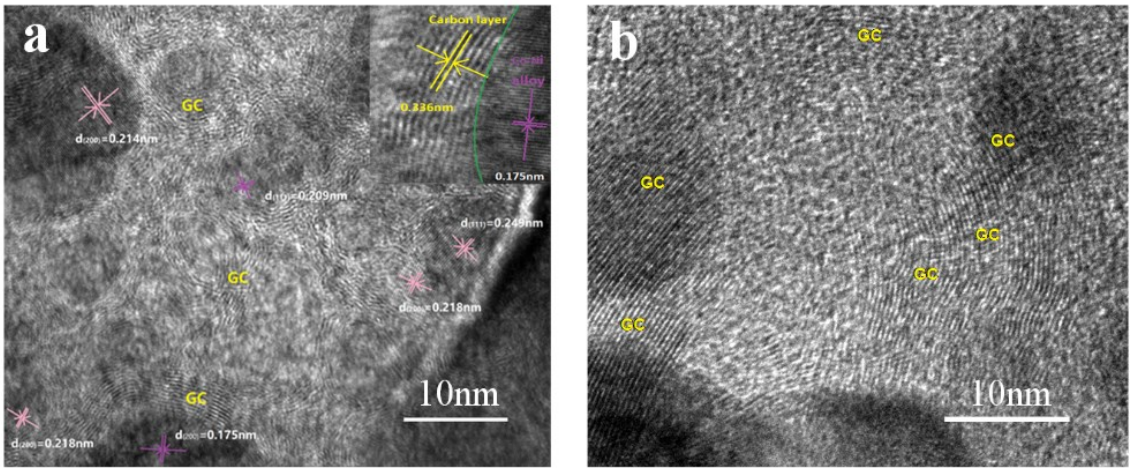

Figure S15. High-resolution TEM images of (a) nanosheet shell belonging to GC-Co@DC-LDO CPs and (b) graphitic carbon core observed from the cross section image prepared by ultramicrotomy. GC means graphitic carbon.

The lattice fringe with d-spacing value of 0.218 nm corresponds to the (200) plane for CoO (or NiO) while 0.175 nm and 0.209 nm corresponded to the (200) and (111) planes for Co (or Ni), respectively.[7]

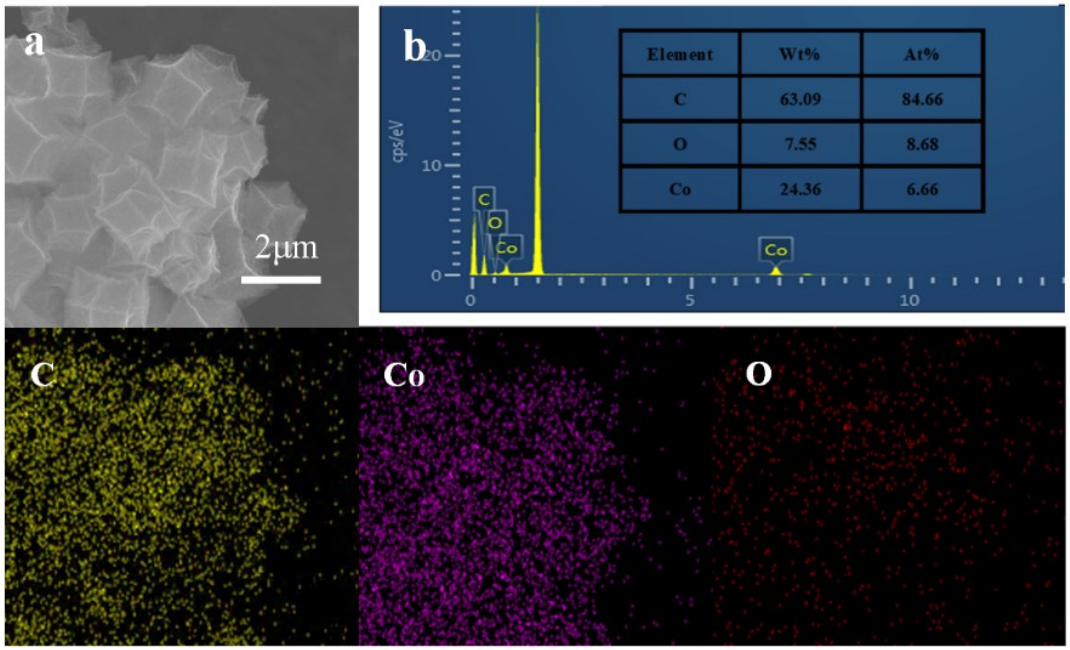

Figure S16. (a) FESEM image and (b) EDX patterns with C, Co, O elemental maps of GC-Co NPs.

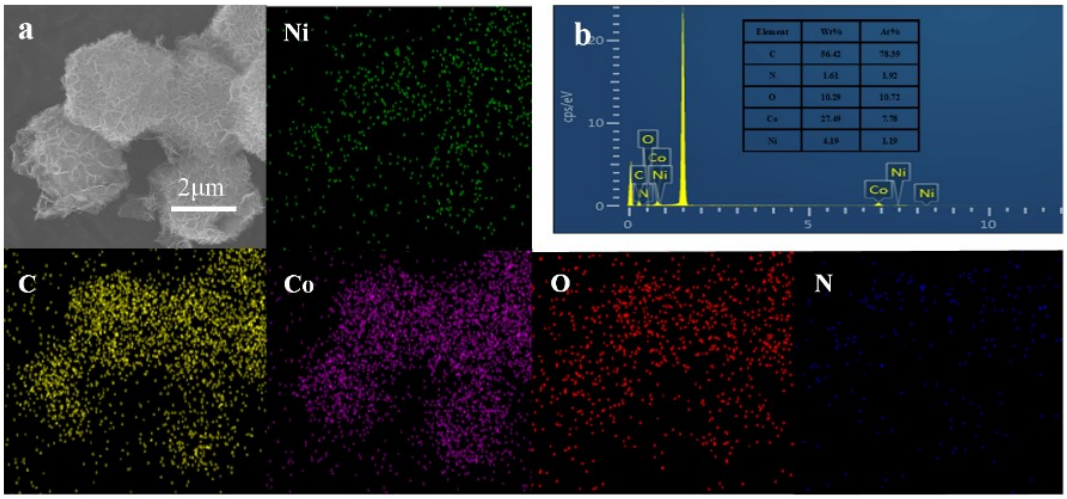

Figure S17. (a) FESEM image and (b) EDX patterns with C, Co, O elemental maps of GC-Co@DC-LDO CPs.

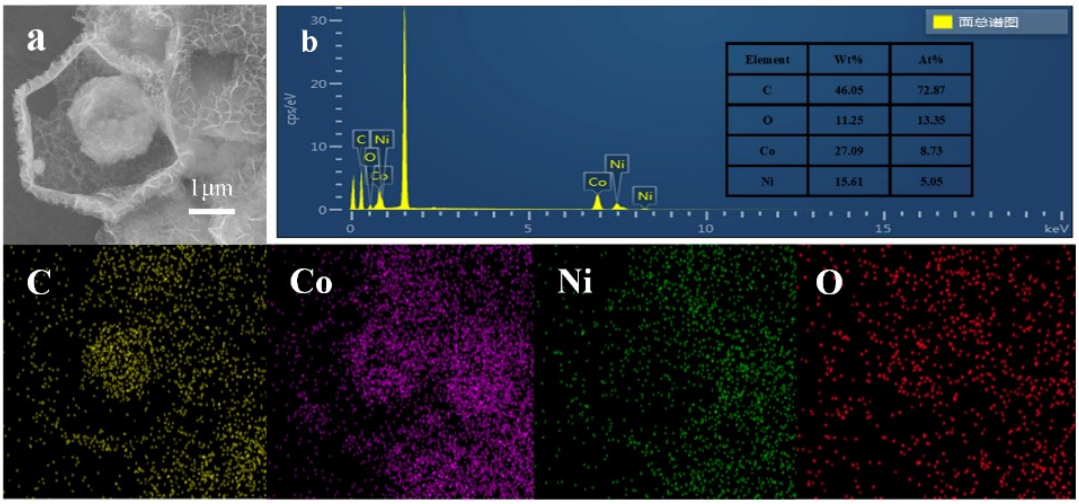

Figure S18. (a) FESEM image and (b) EDX patterns with C, Co, O, Ni elemental maps of GC-Co@DC-LDO YPs.

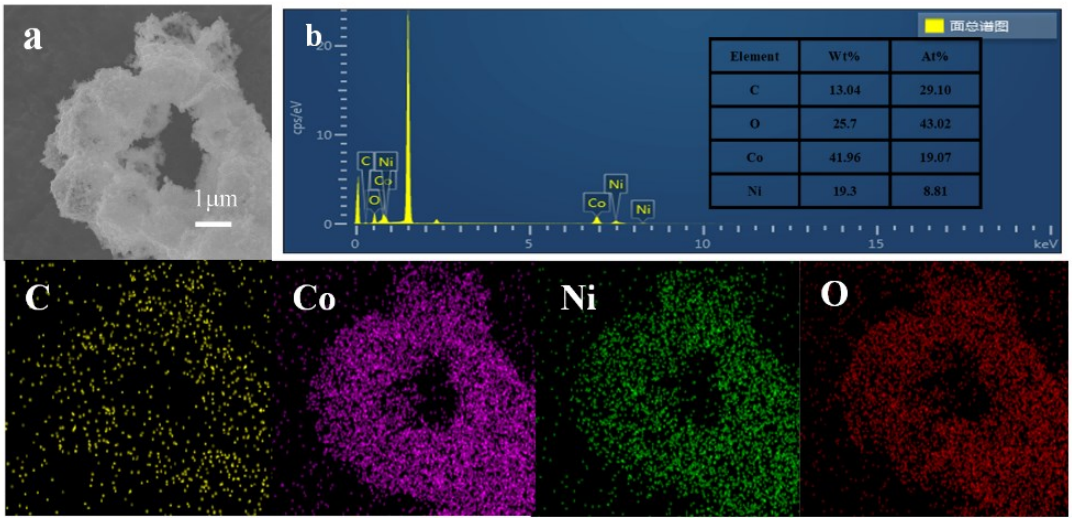

Figure S19. (a) FESEM image and (b) EDX patterns with C, Co, O, Ni elemental maps of LDO HPs.

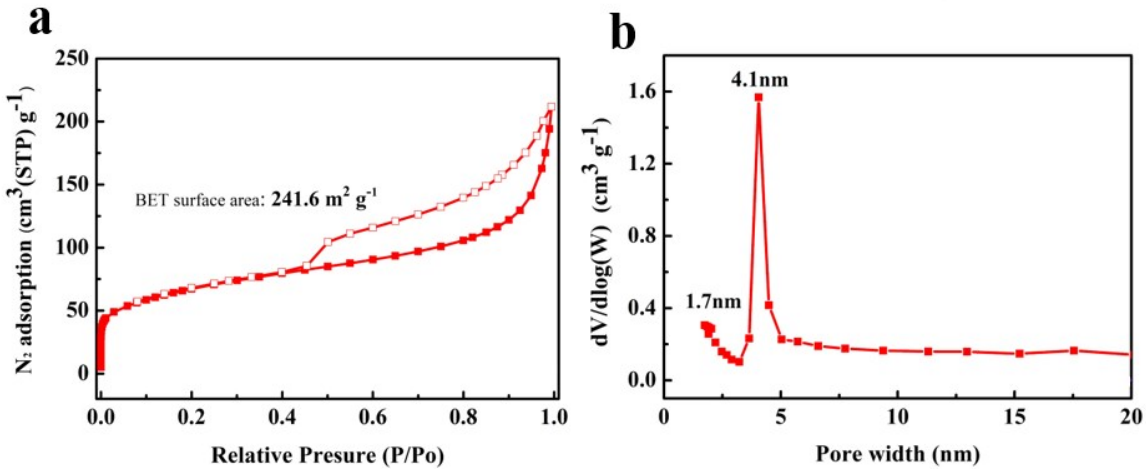

Figure S20. (a) Nitrogen adsorption-desorption isotherms and (b) pore-size distribution of GC-Co@DC-LDO CPs.

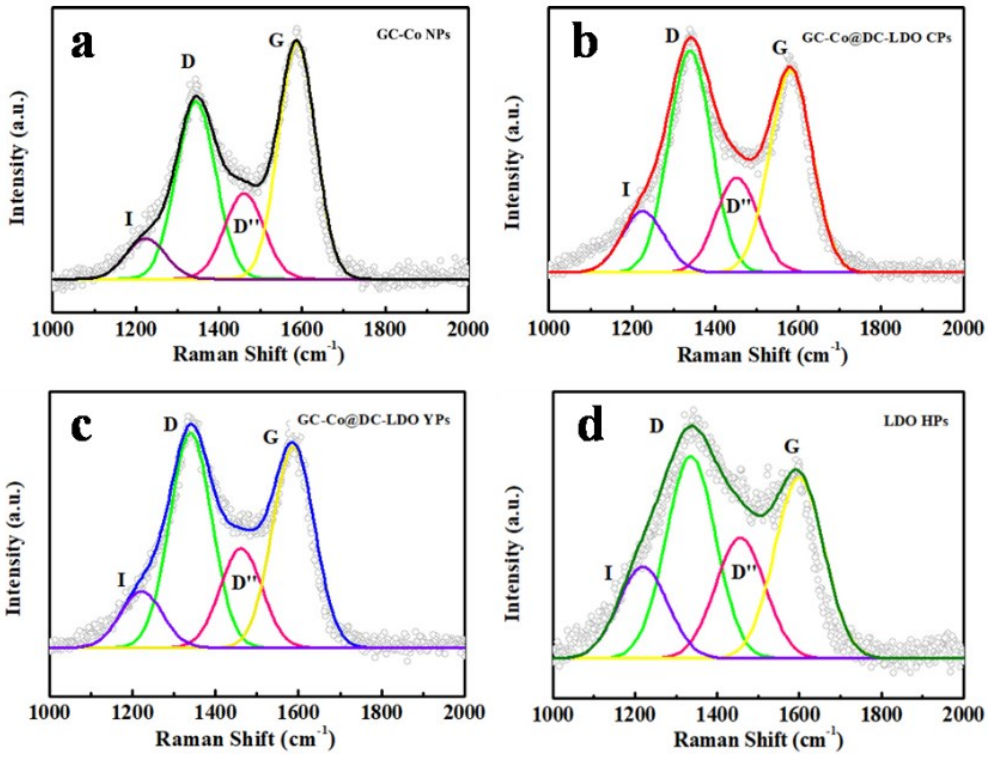

Figure S21. Raman spectra.

The spectra are deconvoluted into four components. The I band is related to the N or other impurities in the graphitic structure. The D" band is an indicator to the stacking disorder of the graphene layer. The 2D band (2672 cm^{-1}), D+G band (2920 cm^{-1}), and 3S band (3195 cm^{-1}) in the Raman spectra come from the carbon frameworks related with second-order zone boundary phonons.[8]

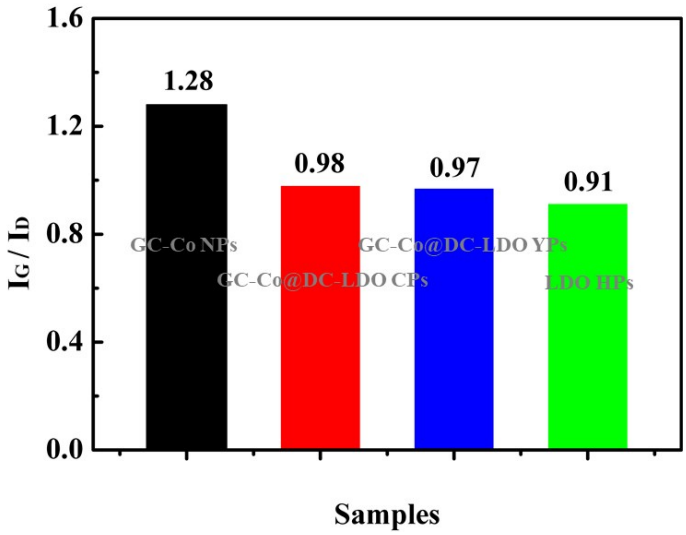

Figure S22. The intensity ratio between G and D bands (I_G/I_D).

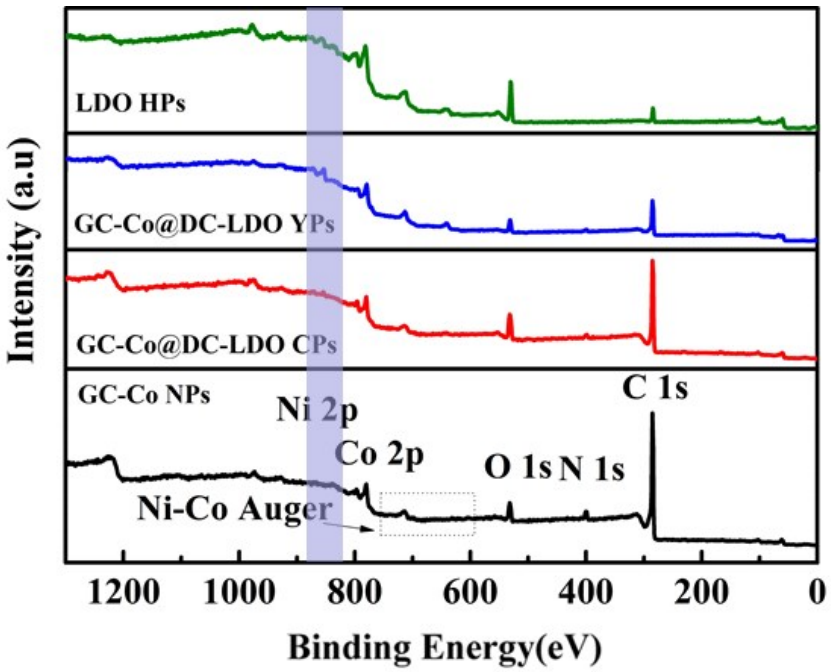

Figure S23. Full XPS spectra of obtained annealed products at 800 ℃.

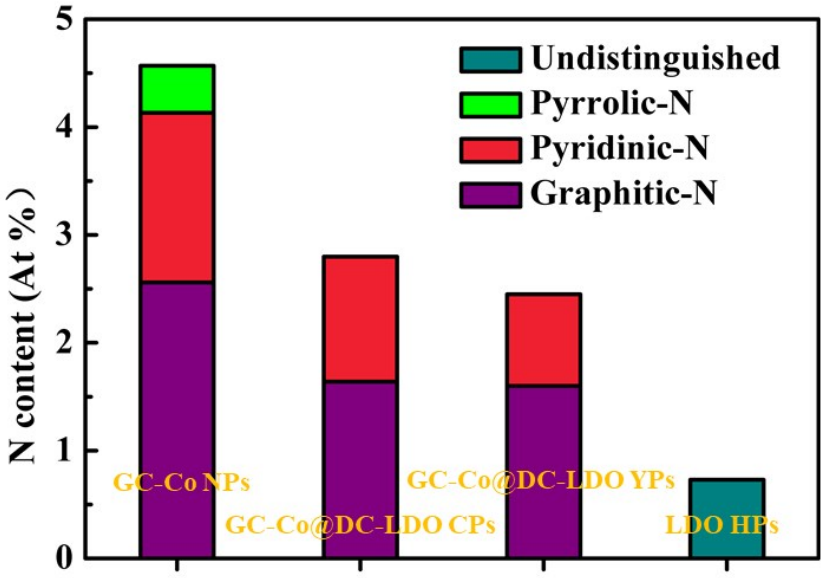

Figure S24. Summary on the N content with XPS detection of obtained annealed products at 800 ℃.

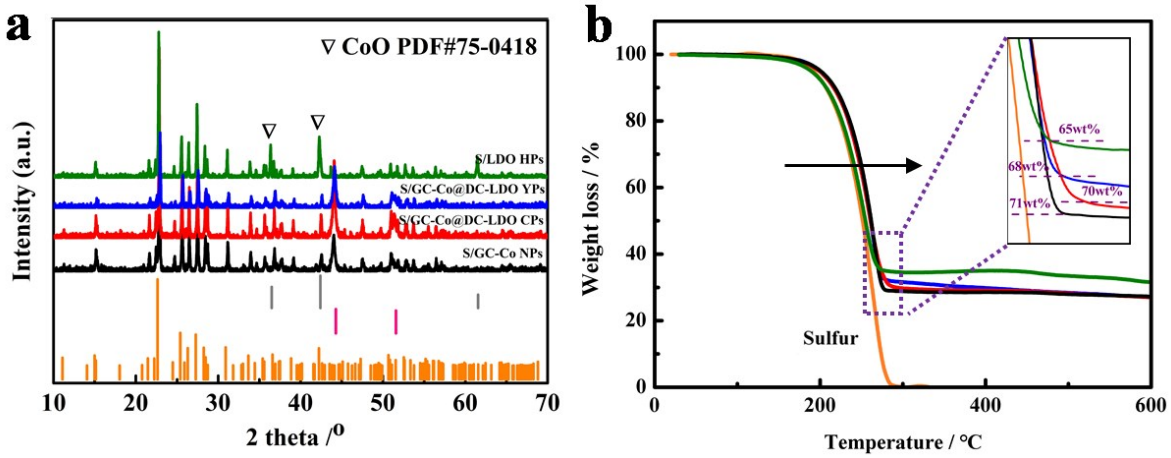

Figure S25. (a) XRD patternsand (b) TGA curves of annealed products loading with sulfur.

The orange line represents pure sulfur: PDF# 85-0799, the pink line represents cubic Co: PDF# 15-0806, and the gray line represents cubic CoO: PDF# 75-0418 in **Figure S20a**.

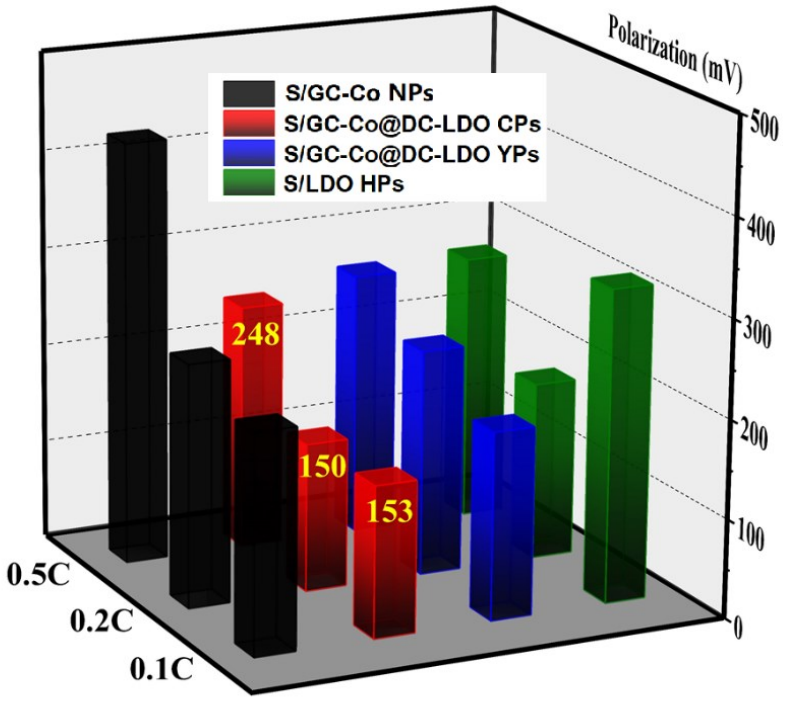

Figure S26. Polarization of different cathodes at the current densities of 0.1, 0.2, and 0.5 C.

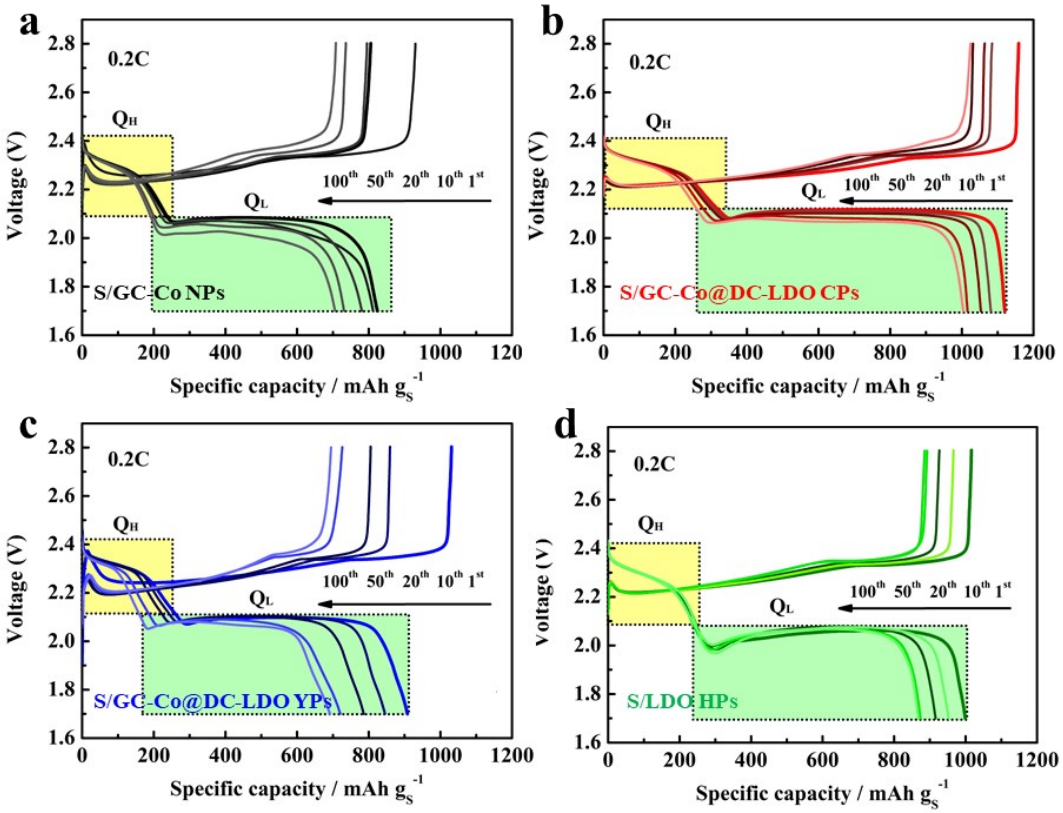

Figure S27. Charge-discharge profiles of Li-S batteries with as-fabricated cathodes at 0.2 C.

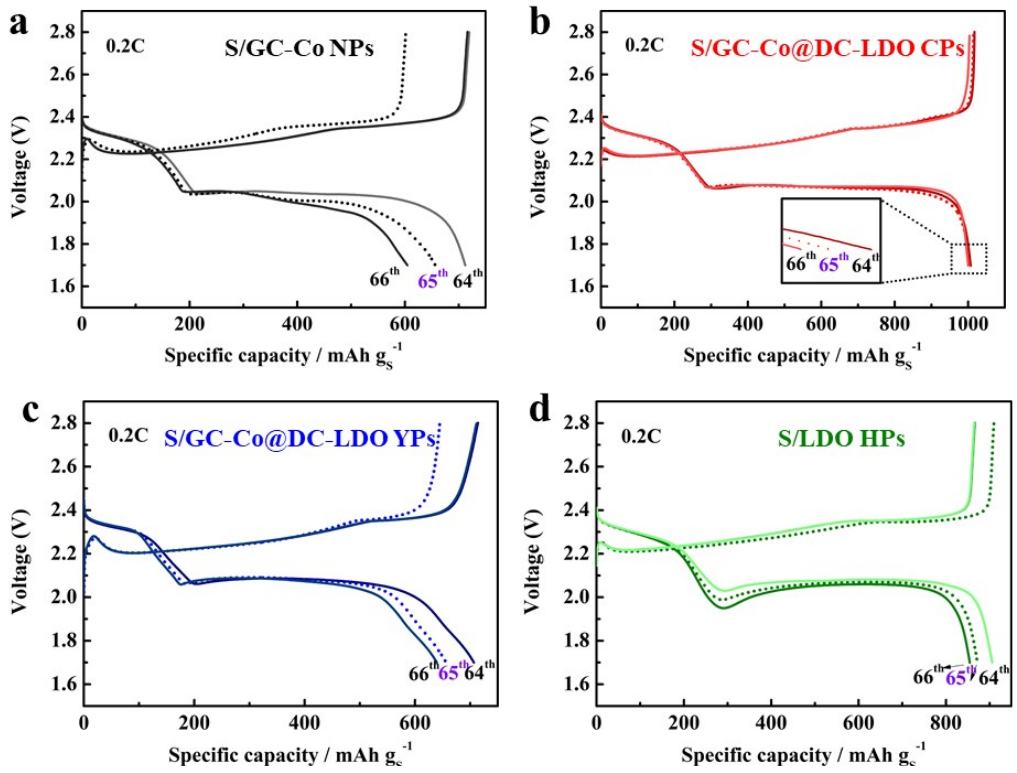

Figure S28. The charge-discharge curves of Li-S batteries with as-fabricated cathodes at 0.2 C before and after 72 h rest.

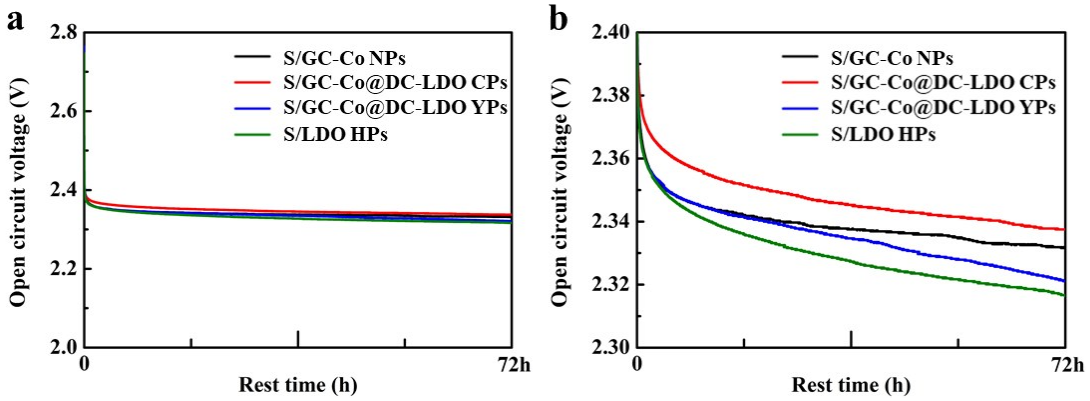

Figure S29. The open-circuit voltage curves of Li-S batteries with as-fabricated cathodes during the 72 h rest.

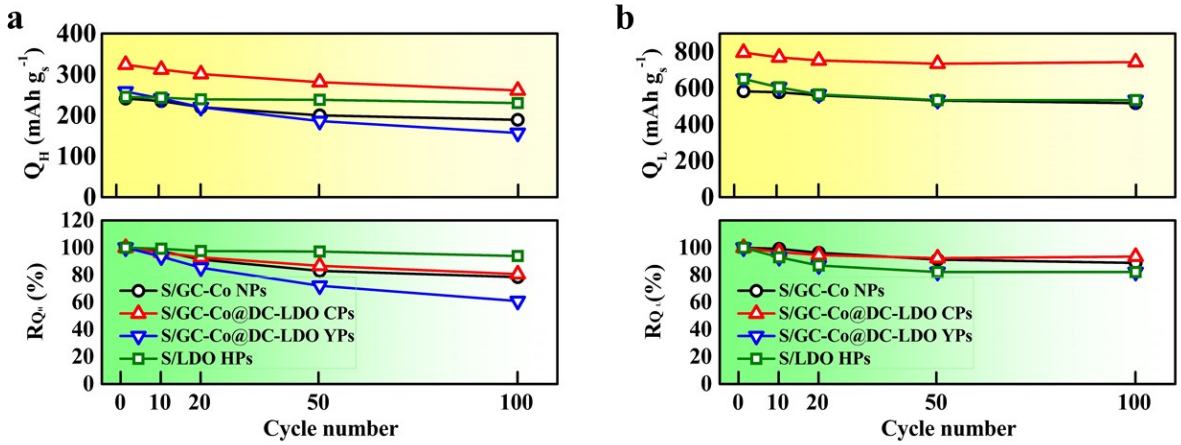

Figure S30. The capacity fading and retention rate of the (a) upper discharge plateaus (Q_H and R_{QH}, respectively) and (b) lower discharge plateaus (Q_L and R_{QL}, respectively).

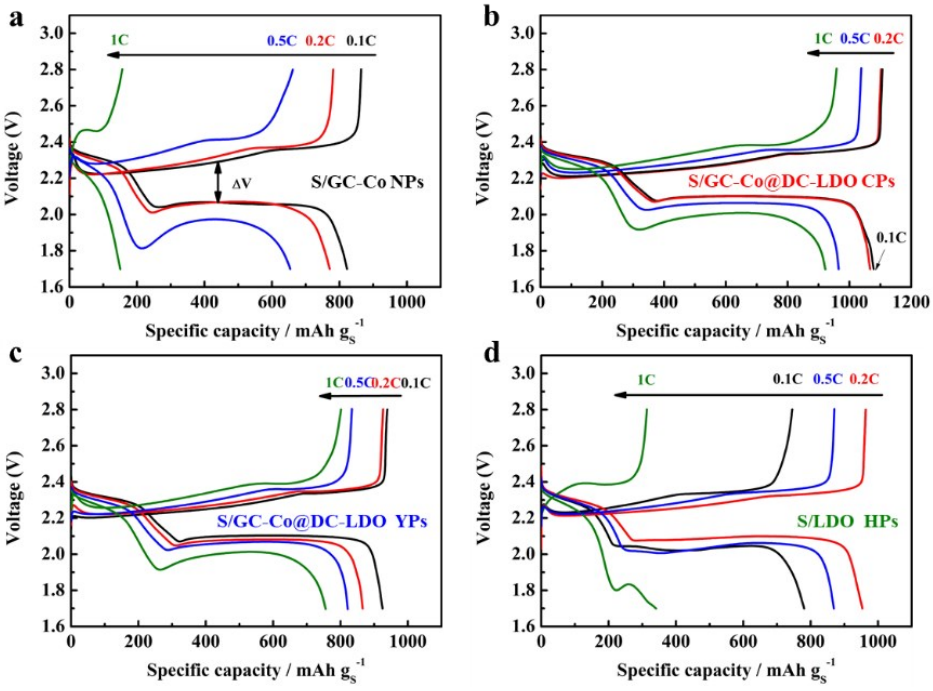

Figure S31. Rate capability of cathodes at various current densities of 0.1-1 C.

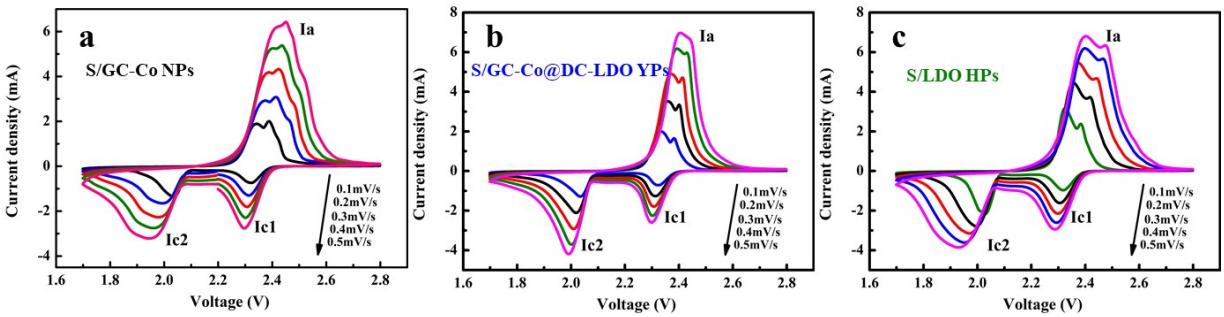

Figure S32. CV curves of cathodes at different scan rates ranging from 0.1 to 0.5 mV s^{-1}.

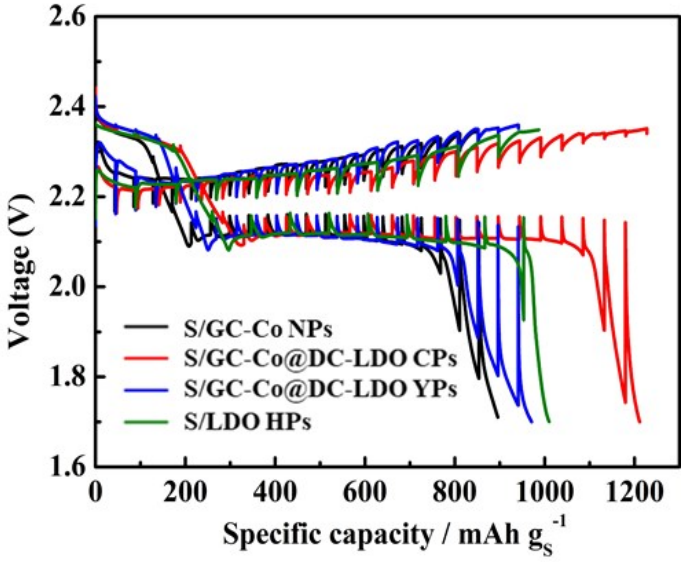

Figure S33. The voltage response curves during GITT measurement.

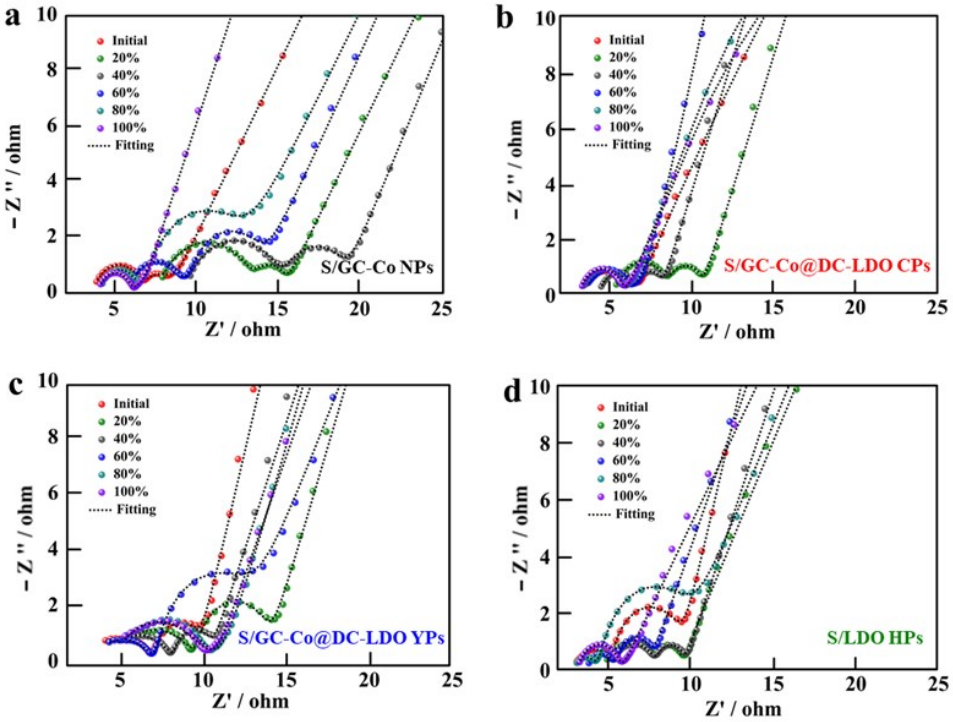

Figure S34. Nyquist plots at different depth of discharge (DOD) with different cathodes.

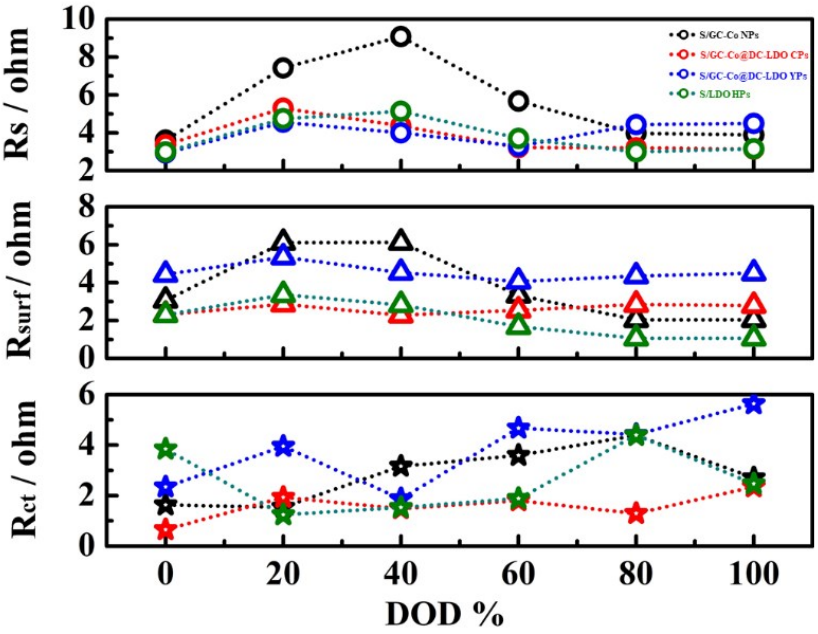

Figure S35. Comparison of R_s, $R_{surf,}$ and R_{ct} for the different four cathodes against DOD.

Table S1. The characterized data of the as-synthesized precursors with different solvothermal durations by ICP-OES and EDX analysis.

Sample	Overall size (μm)	Thickness of shell (nm)	Ni/Co (mass ratio % by ICP-OES)	Ni/Co (mass ratio % by EDX)	N (wt% by EDX)
ZIF-67-90	3	/	/	/	27.9
0.5 H	5.3	/	0.8	Trace	23.8
1 H	6.1	/	0.7	Trace	24.9
1.5 H	6.5	/	4.0	Trace	22.4
2 H (C-ZIF@LDH)	4.3	331	16.5	12.5	20.6
3 H	4.1	395	/	15.6	16.3
4 H	4.9	707	/	29.8	14.1
9H (Y-ZIF@LDH)	5.4	943	30.0	32.9	10.7
12 H	5.4	/	/	43.8	3.4
24 H (H-LDH)	5.5	/	46.7	55.3	1.6

Table S2. The element analysis of C, N, Co and Ni content for the four annealed products (at%). C, Co and Ni content were detected by EDX analysis and N content was detected by XPS analysis.

Sample	C	N	Co	Ni
GC-Co NPs	84.66	4.57	6.66	/
GC-Co@DC-LDO CPs	78.39	2.80	7.78	1.19
GC-Co@DC-LDO YPs	72.87	2.45	8.73	5.05
LDO HPs	29.1	0.73	19.07	8.81

Table S3. The summary of the calculated lithium ion diffusion coefficient. Based on the classical Randles Sevcik equation:

$$I_p = (2.69 \times 10^5)\, n^{1.5}\, A\, D_{Li^+}{}^{0.5} C_{Li}\, V^{0.5}$$

D_{Li^+} ($cm^2\ s^{-1}$)	S/GC-Co NPs ($x10^{-8}$)	S/GC-Co@DC-LDO CPs ($x10^{-8}$)	S/GC-Co@DC-LDO YPs ($x10^{-8}$)	S/LDO HPs ($x10^{-8}$)
A	7.18	10.51	6.36	4.85
C1	1.47	1.29	1.33	1.45
C2	1.24	3.21	1.87	1.03

Table S4. The summary values of R_s, R_{surf}, and R_{ct} for the four cathodes against DOD.

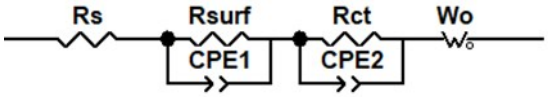

Sample \ R_s /ohm	DOD (%)					
	0	20	40	60	80	100
S/GC-Co NPs	3.61	7.42	9.08	5.67	3.98	3.89
S/GC-Co@DC-LDO CPs	3.37	5.30	4.37	3.22	3.20	3.14
S/GC-Co@DC-LDO YPs	2.93	4.56	4.00	3.29	4.43	4.49
S/LDO HPs	2.99	4.74	5.13	3.73	3.00	3.16

Sample \ R_{surf} /ohm	DOD (%)					
	0	20	40	60	80	100
S/GC-Co NPs	3.06	6.11	6.12	3.33	2.05	2.05
S/GC-Co@DC-LDO CPs	2.32	2.87	2.28	2.54	2.84	2.79
S/GC-Co@DC-LDO YPs	4.44	5.35	4.53	4.07	4.35	4.49
S/LDO HPs	2.38	3.36	2.83	1.69	1.07	1.06

Sample \ R_{ct} /ohm	DOD (%)					
	0	20	40	60	80	100
S/GC-Co NPs	1.63	1.54	3.16	3.59	4.38	2.70
S/GC-Co@DC-LDO CPs	0.65	1.93	1.48	1.80	1.28	2.35
S/GC-Co@DC-LDO YPs	2.34	3.95	1.87	4.67	4.40	5.63
S/LDO HPs	3.85	1.24	1.53	1.88	4.39	2.46

Table S5. Electrochemical performance comparison of Li-S batteries with different catalysts.

Catalyst (Derived from ZIF-67)	0.2 C (Initial capacity) mAh g_s^{-1}	1 C (Initial capacity) mAh g_s^{-1}	1 C (After 400 cycles' capacity) mAh g_s^{-1}	Reference
Co-NCNT/NP	1190	910	815	[9]
CNTs/Co_3S_4−NBs	1330	954	792	[10]
ACNF/Co_3S	1012	953	648	[11]
HPTCF	1210	/	850	[12]
CPZC	1250	1050	830	[13]
NiO-$NiCo_2O_4$@C	1063	1050 (0.5 C)	740 (0.5 C)	[14]
NPC-G	934	700	620 (300 cycles)	[15]
Co_9S_8-3DGF	1100	880	623	[16]
N-CNTs/Co-NFs	1131	1025	730	[17]
ZIF-67-CNTs@NH	/	1030	820	[18]
h-Co-BN-GC	1205	792	783 (200 cycles)	[19]
C-Co/TiO_2	770	870	466 (300 cycle)	[20]
ZDC@ZIF-8	1022	1118	683 (300 cycles)	[21]
CoS_2@NGCNs	1030	680	519 (300 cycles)	[22]
CoP@HPCN-MWCNT	780	700	/	[23]
Co/CoP@NC	1201	1030	730	[24]
H-LDH/Co_9S_8	1063	700	500	[25]
$Ni_xCo_{3-x}S_4$/N-doped carbon	/	1162	532	[26]
GC-Co@DC-LDO CPs	**1140**	**922**	**769**	**This work**

[1] C. Lamiel, V. Nguyen, I. Hussain, J. J. Shim, *Energy* **2017**, *140*, 901.

[2] P. Wang, Y. Li, S. Li, X. Liao, S. Sun, *J. Mater. Sci.: Mater. Electron.* **2017**, *28*, 9221.

[3] Y. Lu, Y. Wang, H. Li, Y. Lin, Z. Jiang, Z. Xie, Q. Kuang, L. Zheng, *ACS Appl. Mater. Interfaces* **2015**, *7*, 13604.

[4] W. P. Kong, J. Li, Y. Chen, Y. Q. Ren, Y. H. Guo, S. L. Niu, Y. Z. Yang, *Appl. Surf. Sci.* **2018**, *437*, 161.

[5] G. Yilmaz, K. M. Yam, C. Zhang, H. J. Fan, G. W. Ho, *Adv. Mater.* **2017**, *29*, 1606814.

[6] a) L. Wang, J. Zhang, Y. Zhu, S. Xu, C. Wang, C. Bian, X. Meng, F.-S. Xiao, *ACS Catal.* **2017**, *7*, 7461;

b) G. L. Tian, M. Q. Zhao, B. S. Zhang, Q. Zhang, W. Zhang, J. Q. Huang, T. C. Chen, W. Z. Qian, D. S. Su, F. Wei, *J. Mater. Chem. A* **2014**, *2*, 1686.

[7] a) Y. N. Liu, J. Y. Zhao, J. T. Feng, Y. F. He, Y. Y. Du, D. Q. Li, *J. Catal.* **2018**, *359*, 251; b) J. Li, S. Lu, H. Huang, D. Liu, Z. Zhuang, C. Zhong, *ACS Sustainable Chem. Eng.* **2018**, *6*, 10021; c) J. P. Hu, J. Chen, H. Lin, R. L. Liu, X. B. Yang, *J. Solid State Chem.* **2018**, *259*, 1.

[8] a) J. J. Duan, S. Chen, M. Jaroniec, S. Z. Qiao, *ACS Nano* **2015**, *9*, 931; b) J. Duan, Y. Zheng, S. Chen, Y. Tang, M. Jaroniec, S. Qiao, *Chem. Commun.* **2013**, *49*, 7705; c) J. Zhang, C. P. Yang, Y. X. Yin, L. J. Wan, Y. G. Guo, *Adv. Mater.* **2016**, *28*, 9539; d) D. Xu, D. Chao, H. Wang, Y. Gong, R. Wang, B. He, X. Hu, H. J. Fan, *Adv. Energy Mater.* **2018**, *8*, 1702769.

[9] T. Chen, B. R. Cheng, G. Y. Zhu, R. P. Chen, Y. Hu, L. B. Ma, H. L. Lv, Y. R. Wang, J. Liang, Z. X. Tie, Z. Jin, J. Liu, *Nano Lett.* **2017**, *17*, 437.

[10] T. Chen, Z. Zhang, B. Cheng, R. Chen, Y. Hu, L. Ma, G. Zhu, J. Liu, Z. Jin, *J. Am. Chem. Soc.* **2017**, *139*, 12710.

[11] H. Xu, A. Manthiram, *Nano Energy* **2017**, *33*, 124.

[12] W. Cai, G. Li, D. Luo, G. Xiao, S. Zhu, Y. Zhao, Z. Chen, Y. Zhu, Y. Qian, *Adv. Energy Mater.* **2018**, *8*, 1802561.

[13] G. Li, W. Lei, D. Luo, Y. Deng, Z. Deng, D. Wang, A. Yu, Z. Chen, *Energy Environ. Sci.* **2018**, 11, 2372.

[14] L. Hu, C. Dai, H. Liu, Y. Li, B. Shen, Y. Chen, S. J. Bao, M. Xu, *Adv. Energy Mater.* **2018**, *8*, 1800709.

[15] K. Chen, Z. Sun, R. Fang, Y. Shi, H. M. Cheng, F. Li, *Adv Funct Mater* **2018**, *28*, 1707592.

[16] J. He, Y. Chen, A. Manthiram, *iScience* **2018**, *4*, 36.

[17] L. Ma, H. Lin, W. Zhang, P. Zhao, G. Zhu, Y. Hu, R. Chen, Z. Tie, J. Liu, Z. Jin, *Nano Lett.* **2018**, *18*, 7421.

[18] H. Wu, Y. Li, J. Ren, D. Rao, Q. Zheng, L. Zhou, D. Lin, *Nano Energy* **2019**, *55*, 82.

[19] N. Li, K. Chen, S. Chen, F. Wang, D. Wang, F. Gan, X. He, Y. Huang, *Carbon* **2019**, *149*, 564.

[20] R. Liu, Z. Liu, W. Liu, Y. Liu, X. Lin, Y. Li, P. Li, Z. Huang, X. Feng, L. Yu, D. Wang, Y. Ma, W. Huang, *Small* **2019**, e1804533.

[21] T. Pan, Z. Li, Q. He, X. Xu, L. He, J. Meng, C. Zhou, Y. Zhao, L. Mai, *Energy Storage Mater.* **2019**, 15, 1804533.

[22] S. D. Seo, D. Park, S. Park, D. W. Kim, *Adv. Funct. Mater.* **2019**, *29*, 1903712.

[23] Z. Ye, Y. Jiang, J. Qian, W. Li, T. Feng, L. Li, F. Wu, R. Chen, *Nano Energy* **2019**, *64*, 103965.

[24] Y. Li, P. Xu, G. Chen, J. Mou, S. Xue, K. Li, F. Zheng, Q. Dong, J. Hu, C. Yang, M. Liu, *Chem. Eng. J.* **2020**, *380*, 122595.

[25] S. H. Chen, J. H. Luo, N. X. Han, W. Jun, D. Qiang, Z. L. Zeng, S. G. Deng, Energy Storage Mater. **2020**, *30*, 187-195.

[26] X. B. Liao, Z. H. Li, H. Qiu, L. X. Xia, Y. Li, S. H. Zhu, M. M. Wang, H. Wang, X. Xu, L. Q. Mai, Y. Zhao, *ACS Appl. Mater. Interfaces* **2020***, 12*, 9181-9189.